Tozuka *et al.*
Progress in Earth and Planetary Science (2022) 9:70
https://doi.org/10.1186/s40645-022-00532-0

Progress in Earth and Planetary Science

RESEARCH ARTICLE

Open Access

Simulated decadal variations of surface and subsurface phytoplankton in the upstream Kuroshio Extension region

Tomoki Tozuka[1,2*], Yoshikazu Sasai[3], Sayaka Yasunaka[4], Hideharu Sasaki[2] and Masami Nonaka[2]

Abstract

Using outputs from an ecosystem model embedded in an eddy-resolving ocean general circulation model that can realistically simulate decadal modulations of the Kuroshio Extension (KE) between stable and unstable states, decadal variations of phytoplankton concentration in the upstream KE region are investigated. During stable states of the KE, surface phytoplankton concentrations are anomalously suppressed to the south of the KE front, while those to the north are anomalously enhanced. Although the surface phytoplankton concentration anomalies are prominent only during winter to spring, significant subsurface anomalies centered around 60 m depth persist even in summer and autumn. Anomalies persist throughout the year in phytoplankton biomass integrated over the upper 100 m despite the strong surface anomalies during the spring bloom season. An analysis of nitrogen concentration anomalies suggests that the vertical movement of the isopycnal surfaces, vertical mixing of nutrients, and meridional shifts in the KE jet contribute to the anomalous phytoplankton biomass.

Keywords: Phytoplankton, Kuroshio Extension, Decadal variation, Ecosystem model, Eddy-resolving ocean general circulation model

1 Introduction

The Kuroshio Extension (KE) in the northwestern Pacific undergoes large decadal variations and is known to shift between stable and unstable states (Qiu and Chen 2005). It has been shown that wind stress curl anomalies in the central North Pacific that excite Rossby waves (Latif and Barnett 1996; Qiu and Chen 2005; Taguchi et al. 2007; Nonaka et al. 2006; Qiu et al. 2014) are the root cause of this decadal variability. When these Rossby waves reach the KE, they are trapped along the jet and lead to a stable state when downwelling Rossby waves impinge and an unstable state when upwelling Rossby waves arrive (Sasaki and Schneider 2011; Sasaki et al. 2013).

To understand how such decadal variations in the KE affect marine ecosystem, which are also known to undergo large decadal variations (Noto and Yasuda 1999; Chiba et al. 2013), it is necessary to understand decadal variations in the lower trophic level marine ecosystem. In this regard, Lin et al. (2014) investigated decadal variations in surface chlorophyll associated with decadal modulations of the KE using satellite data. They revealed that the surface chlorophyll south of 35°N becomes anomalously low when the KE is in the stable state, while it increases anomalously during the KE unstable state. In some extreme years, anomalies can reach up to 35% compared to the climatological value during the spring bloom season. They suggested that anomalous vertical nutrient supply induced by westward propagating Rossby waves related to the North Pacific Gyre Oscillation (Di Lorenzo et al. 2008) and Pacific Decadal Oscillation (Mantua et al. 1997; Newman et al. 2016) contributes to the decadal surface chlorophyll variations. Lin et al. (2020)

*Correspondence: tozuka@eps.s.u-tokyo.ac.jp

[1] Department of Earth and Planetary Science, Graduate School of Science, The University of Tokyo, Tokyo, Japan
Full list of author information is available at the end of the article

later successfully reproduced the above decadal variations with their coupled physical–biological model and conducted a mixed layer nitrogen budget analysis. It is shown that the vertical advection mainly caused by nutricline heaving plays an important role. However, their analyses mostly focused on the impacts of the decadal variations of the KE on the surface chlorophyll in the annual mean and the spring bloom. Since chlorophyll a (Chl-a) often retains its maximum in the subsurface layer in this region (Fujiki et al. 2020; Yasunaka et al. 2022), it will be illuminating to also examine subsurface variability for more comprehensive understanding.

This paper is organized as follows. A brief description of the model and datasets used in this study is provided in the next section. In Sect. 3, simulated seasonal variations in phytoplankton are described first, which is a prerequisite to understand decadal variations. Then, simulated surface and subsurface phytoplankton concentration anomalies during the KE stable state are presented and their possible mechanisms are discussed. Conclusions and discussions are given in the final section.

2 Methods

2.1 Model

We have used outputs from a simple nitrogen-based NPZD (nitrogen, phytoplankton, zooplankton, and detritus) pelagic model (Oschlies 2000) embedded in an eddy-resolving ocean general circulation model called the Ocean general circulation model For the Earth Simulator (OFES2) (Masumoto et al. 2004; Sasaki et al. 2020; Sasai et al. 2006, 2007a, 2007b, 2010, 2022) configured for the North Pacific. The horizontal resolution is $0.1^\circ \times 0.1^\circ$, and there are 105 levels in the vertical. The physical fields are spun up with the monthly climatology of the JRA55-do (Tsujino et al. 2018) for 50 years and are forced by the 3-hourly data of the JRA55-do from 1958 to 1979. The last day of 1979 is used in initial physical conditions for the coupled physical-biological model, and then, it is forced from 1980 to 2019. In this study, we have used 40-year outputs of the coupled physical-biological model from 1980 to 2019. For more details about this ecosystem model embedded in the eddy-resolving model including its more thorough validations in the North Pacific, readers are referred to a paper by Sasai et al. (2022).

2.2 Data

To validate the model simulation, we use daily satellite altimetry data for sea surface height (SSH), which was downloaded from the Copernicus Climate Data Store. It covers the period from 1993 to 2019, and its horizontal resolution is $0.25^\circ \times 0.25^\circ$. Also, we use a high-resolution data-assimilation product known as the four-dimensional variational ocean re-analysis for the Western North Pacific over 30 years (FORA-WNP30) (Usui et al. 2017). It is based on the Meteorological Research Institute (MRI) Community Ocean Model version 2.4 (Tsujino et al. 2006), and the four-dimensional variational analysis scheme version of the MRI Multivariate Ocean Variational Estimation system (Usui et al. 2015) is used. The horizontal resolution is $0.1^\circ \times 0.1^\circ$, and we use the product from 1982 to 2015. Subsurface Chl-a data are obtained from the World Ocean Database 2018 (WOD2018; Boyer et al. 2018) and the Global Ocean Data Analysis Project version 2.2019 Release (GLODAPv2.2019; Olsen et al. 2019). Monthly mean Chl-a concentrations with a horizontal resolution of $1^\circ \times 1^\circ$ are calculated at 10 different vertical levels in the upper 200 m (see Yasunaka et al. (2022) for more details). The World Ocean Atlas 2018 (WOA2018; Garcia et al. 2018) is used for nitrate concentration, while Mixed Layer data set of Argo, Grid Point Value (MILA GPV; Hosoda et al. 2010) based on the Argo profiles is used for mixed layer depth (MLD). The horizontal resolution is $1^\circ \times 1^\circ$ for both datasets. The data-derived euphotic layer is estimated from the satellite-based photosynthetically available radiation (PAR) and 1% light level depth from the GlobColour project website (GlobColour_R2018; Frouin et al. 2003; Morel et al. 2007) (see Yasunaka et al. (2022) for more details).

3 Results

The study area of this paper is schematically shown in Fig. 1. The Kuroshio that flows along the southern coast of Japan separates from the coast and flows into the interior ocean of the North Pacific as the KE. Horizontally, nutrients are rich on the northern side of the KE and poor on the southern side, while in the vertical direction, nutrient-rich water is found at depth, which may be brought to the surface mixed layer by vertical mixing. The shortwave radiation from the sun penetrates into the ocean, and it is sufficient to support photosynthesis of phytoplankton in the euphotic layer.

3.1 Seasonal variation

Prior to investigating decadal variations in phytoplankton concentrations, it is necessary to understand its seasonal characteristics (Tozuka et al. 2017). Figure 2a shows the climatology of phytoplankton concentration simulated in the upstream KE region averaged between 142°E and 153°E. As expected, the phytoplankton concentration is much higher to the north of the KE jet throughout the year and reaches its maximum in the spring bloom season in April. Although the maximum is located at the surface from December to April, the maximum appears in the subsurface centered around 60 m depth from June to October (Fig. 2a). This is

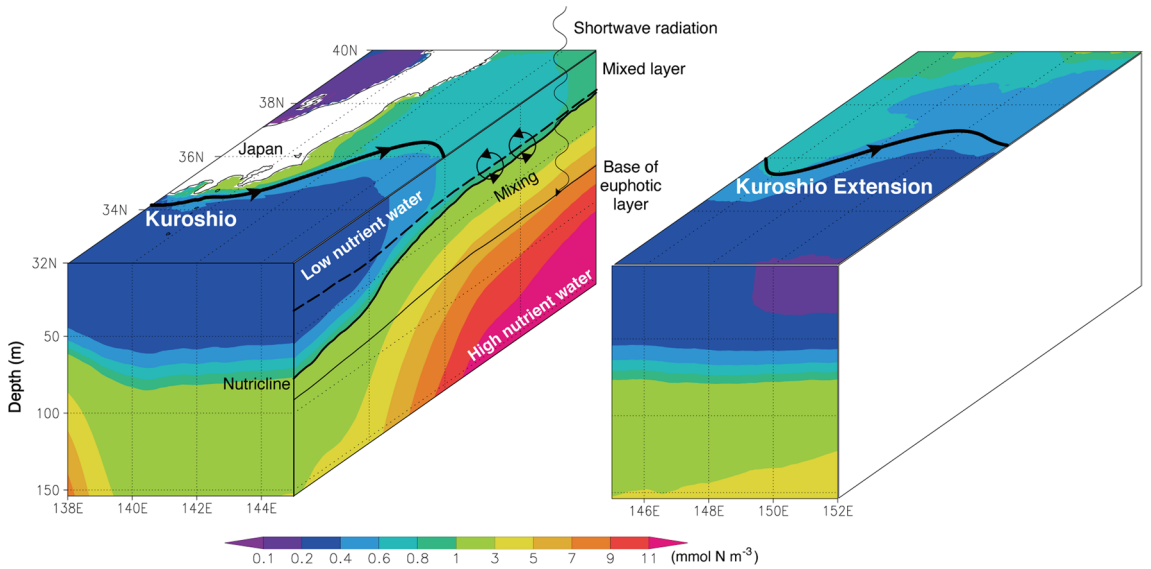

Fig. 1 Schematic diagram of the study area showing three-dimensional structure of nitrogen concentration as well as the major circulation pattern and relevant processes/layers. For nitrogen concentration (shading), nutricline (thick solid line), mixed layer depth (thick dashed line), and the base of euphotic layer (thin solid line), the climatological mean of October from the OFES are used

because nitrogen is depleted after the spring bloom in the surface mixed layer, defined by the depth at which the potential density increases by 0.03 kg m^{-3} from its surface value, but sufficient nitrogen is found in the subsurface even in summer and autumn (nutricline defined by the depth of 1 mmol N m^{-3} isoline is deeper than the mixed layer) and the euphotic layer (i.e., the depth of the 1 W m^{-2} irradiance; Pastor et al. 2013) is deep enough. Such a subsurface maximum is seen in the observed Chl-a concentration in summer/autumn, although the maximum is located at shallower depths to the north of the KE jet and a deeper level to the south of the KE jet (Fig. 2b; Itoh et al. 2015; Yasunaka et al. 2022). Also, the vertical migration of the simulated nutricline is in agreement with the observation (Fig. 2); more specifically, the nutricline outcrops in February, but it deepens from April to October and starts to outcrop again to the north of the KE jet in December. Furthermore, the euphotic layer depth in both the model and observational estimates decreases with latitude and reaches its seasonal maximum in summer with stronger shortwave radiation, although the depth tends to be deeper in the model, especially from December to April. Since subsurface observations of Chl-a concentrations are still limited, Fig. 2b is noisier than Fig. 2a and data are missing in some months. For this reason, the observational subsurface Chl-a data is used only to validate the simulated seasonal variations.

3.2 Decadal variations

To define the stable and unstable states of the KE, we have first applied an empirical orthogonal function (EOF) analysis to SSH anomalies in 140°E-170°E, 30°N-40°N following Sasaki et al. (2013). The first EOF mode successfully captures the well-known decadal modulations of the KE between stable and unstable states; i.e., SSH anomalies with opposite signs are found to the south and north of the KE jet (Fig. 3a). This leading mode explains 14.8% of the total variance. Based on the criterion of North et al. (1982), it is significantly separated from the second EOF mode, whose variance contribution is 7.4%. The spatial distribution and variance contribution are consistent with those obtained from the same analysis with the satellite observation (Fig. 3b) and FORA (Fig. 3c).

We have then computed the annual mean value of the first principal component (PC) (Fig. 3d). The PC obtained from the model is well correlated with those from satellite observations and FORA with their correlation coefficients of 0.70 and 0.62, respectively. The relatively high correlations not only suggest that the model has high skill in simulating decadal variability in the KE, but also indicate that decadal fluctuations in SSH over the KE have a deterministic component with respect to atmospheric forcing (Qiu et al. 2014). The first PC without any temporal filter undergoes large decadal variations with its value above 1 standard deviation in eight years (1990, 2002, 2003, 2004, 2005, 2011, 2015, and 2018) and below -1 standard deviations in eight years (1983, 1985, 1986, 1996, 1997, 1998, 2007, and 2008). These years are

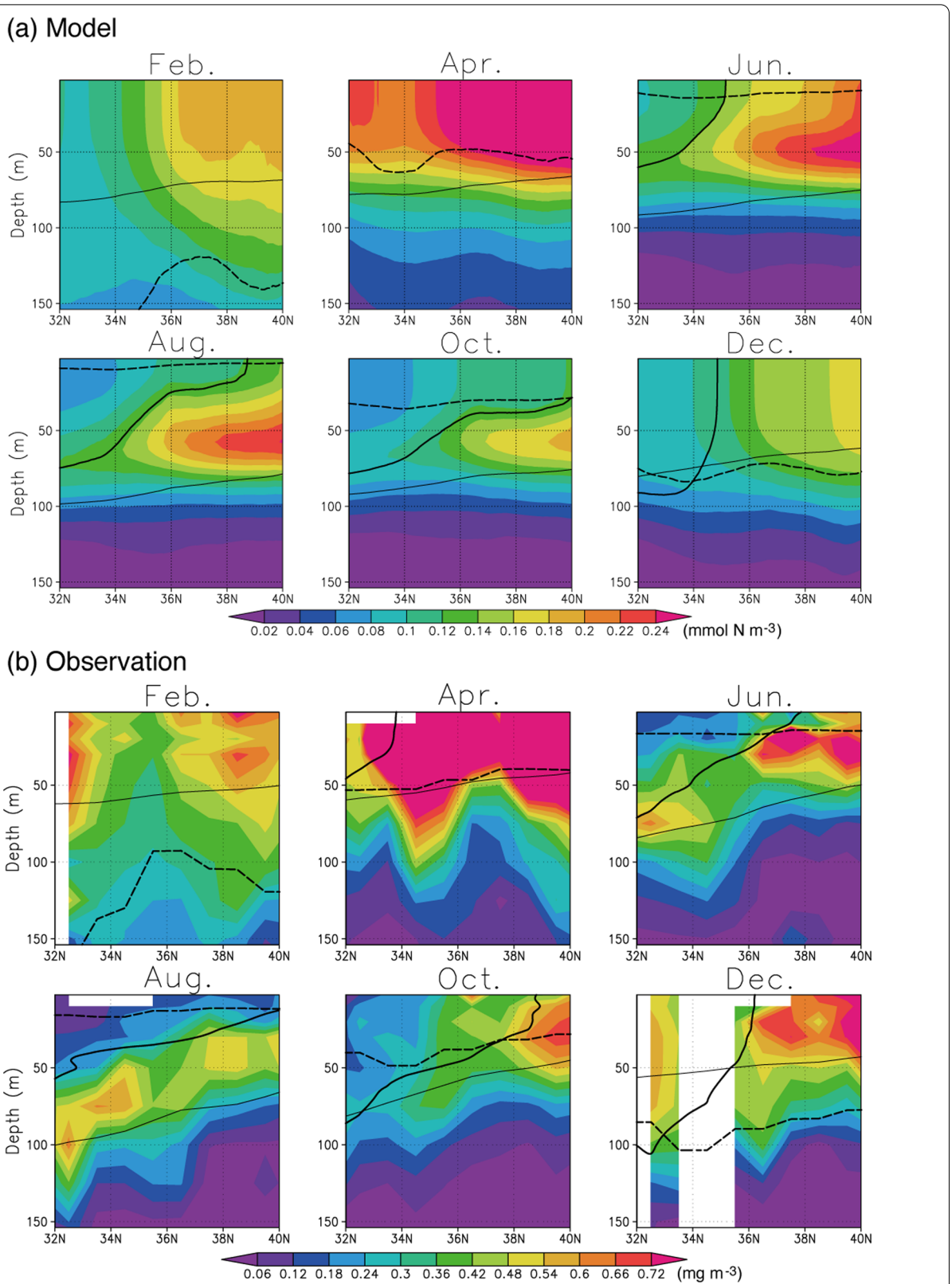

Fig. 2 Monthly climatology of phytoplankton concentration in the upstream Kuroshio Extension (KE) averaged between 142°E and 153°E for **a** OFES2 and **b** observation. The thick solid lines represent nutricline, the thick dashed lines represent the base of the mixed layer, and the thin solid lines represent the base of euphotic layer

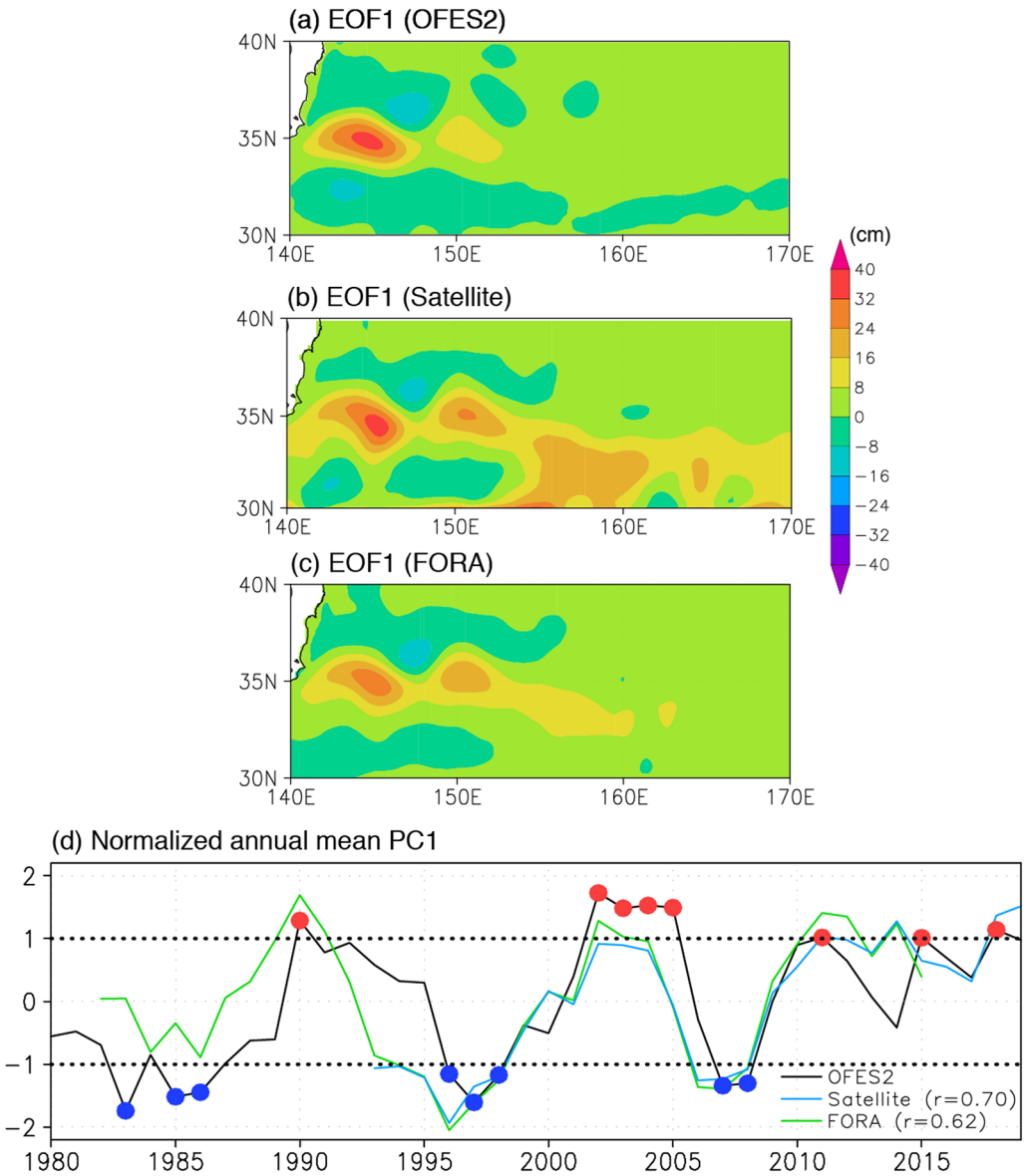

Fig. 3 First empirical orthogonal function (EOF) mode of sea surface height (SSH) anomalies in 140°E-170°E, 30°N-40°N obtained from **a** OFES2, **b** satellite observation, and **c** FORA. **d** Normalized annual mean of the first principal component (PC) of SSH anomalies in 140°E-170°E, 30°N-40°N obtained from the OFES2 (black line), satellite observation (light blue line), and FORA (green line). The horizontal black dotted lines represent ±1 standard deviation, and the red (blue) dots represent the stable (unstable) states

defined, respectively, as the stable and unstable states. Since the unstable state is close to a mirror image of the stable state in general, we focus on the stable state in this study.

To investigate decadal variations in phytoplankton concentrations and their controlling mechanisms, composites of their surface anomalies during stable states are constructed (Fig. 4). Throughout the year, negative phytoplankton concentration anomalies are found to the south of the KE jet, while positive anomalies are found to the north, but these anomalies are more conspicuous during winter and spring. The results are consistent with those of Lin et al. (2014, 2020).

To examine whether such anomalies are also found in the subsurface, composites of phytoplankton concentration anomalies along 145°E, where the strongest surface negative anomalies are found to the south of KE in winter, are prepared (Fig. 5). It is clear that significant phytoplankton concentration anomalies are not confined to the surface, but extend down to around 100 m depth in

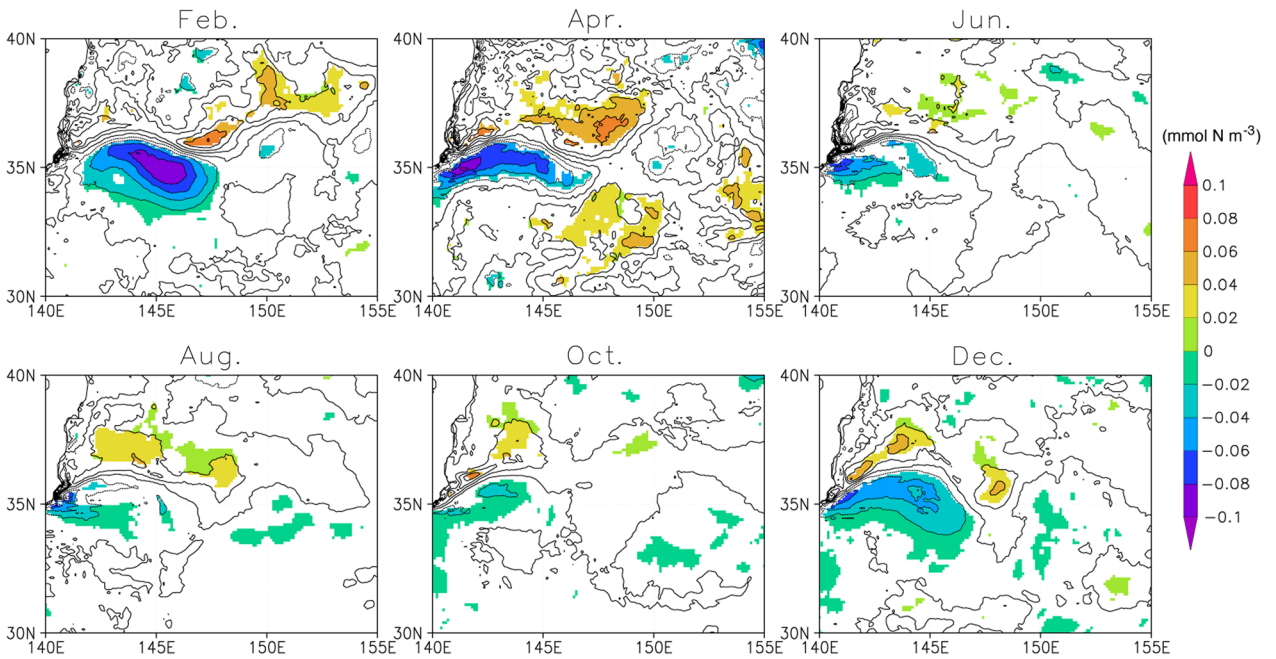

Fig. 4 Composites of phytoplankton concentration anomalies at the surface during the stable states. The contour intervals are 0.02 mmol N m^{-3}. Anomalies significant at the 95% confidence level by a two-tailed t test are shaded

winter to the south of the KE jet located around 36°N. It is intriguing that significant phytoplankton concentration anomalies remain in the subsurface layer even in August and October despite the disappearance of significant anomalies near the surface during these months. As a result, significant anomalies exist throughout the year in the phytoplankton biomass integrated over the upper 100 m even though the strong surface anomalies are found during the spring bloom season (Fig. 6). Thus, the decadal variations of the KE may have larger impacts on marine ecosystems and carbon dioxide uptake than previously thought, as the impacts are not limited to the spring bloom season.

To understand the mechanism of this interesting seasonal evolution of phytoplankton concentration anomalies, we have constructed composites of nitrogen concentration anomalies along 145°E. Figure 7a reveals that significant negative concentration anomalies extend to the surface south of the KE jet throughout the year. This may explain why phytoplankton concentrations decreased anomalously to the south of the KE jet during stable states. Since the climatological mean nitrogen concentration is already too low to sustain the phytoplankton activity near the surface in summer and autumn, nitrogen concentration anomalies do not lead to significant phytoplankton concentration anomalies during these two seasons.

To check the relative importance of anomalous vertical movement of the isopycnal surfaces and vertical mixing of nitrogen, composites of nitrogen concentration anomalies in a density coordinate are examined (Fig. 7b). If the vertical process were important as suggested by Lin et al. (2020) and nitrogen concentration anomalies were solely due to vertical shifts in the nutricline, we would expect significant anomalies to disappear in the density coordinate. However, we find significant but weaker nitrogen concentration anomalies throughout the year. This suggests that adiabatic vertical movements make a substantial contribution, but diapycnal mixing also plays a role in the negative nitrogen and phytoplankton concentration anomalies to the south of the KE jet. We note that phytoplankton concentration anomalies may also contribute to nitrogen concentration anomalies through consumption, but negative phytoplankton concentration anomalies are expected to lead to less consumption of nitrogen and cannot explain the negative anomalies in the nitrogen concentration.

We suggest two possible mechanisms explaining how vertical movements and mixing contribute to the negative nitrogen concentration anomalies to the south of the KE jet during the KE stable state. First, positive anomalies in the vertical gradient of nitrogen concentration (i.e., negative nitrogen concentration anomalies are smaller near the surface) (Fig. 7a) lead to a reduced supply by the vertical movement and mixing. Second,

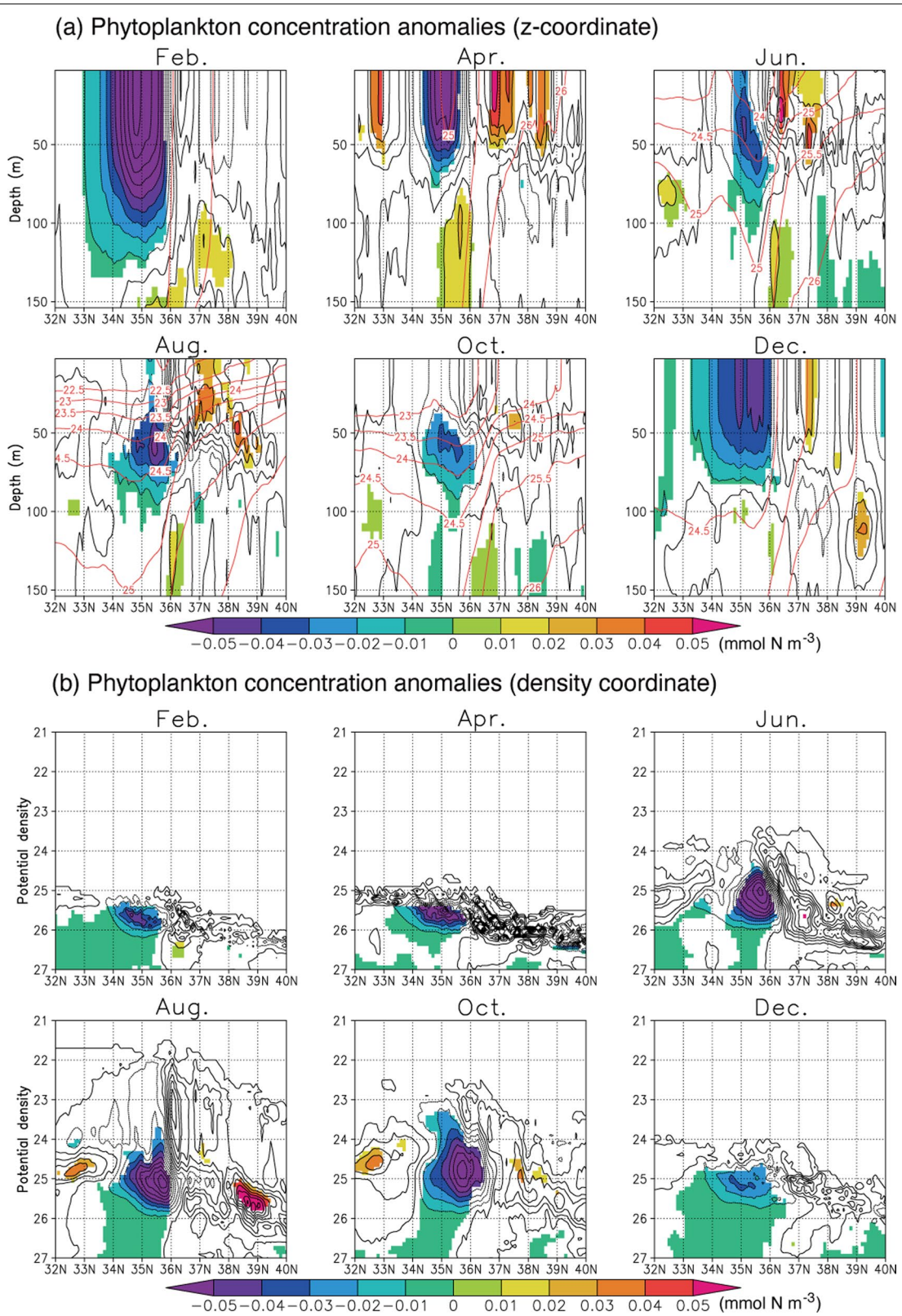

Fig. 5 Composites of phytoplankton concentration anomalies (in mmol N m^{-3}) along 145°E in the upstream KE during the stable states in **a** the z-coordinate and **b** the density coordinate. The black contour intervals are 0.01 mmol N m^{-3}. Also shown in (**a**) with red contours are composites of potential density. Anomalies significant at the 95% confidence level by a two-tailed t test are shaded

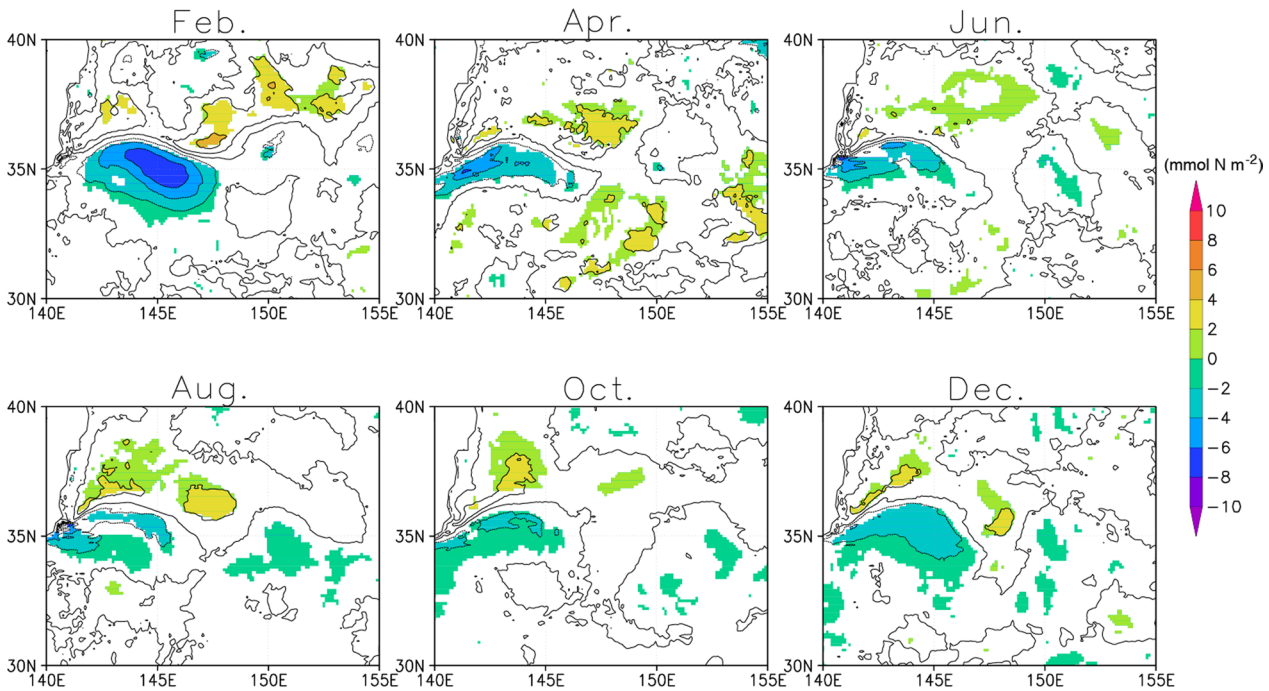

Fig. 6 Composites of phytoplankton concentration anomalies integrated over the upper 100 m. The contour intervals are 2 mmol N m^{-2}. Anomalies significant at the 95% confidence level by a two-tailed t test are shaded

downwelling anomalies to the south of the KE jet also lead to less upward transport of nitrogen-rich water from the subsurface.

Furthermore, when the KE jet latitude coordinate is used, the nitrogen concentration anomalies become smaller in amplitude (Fig. 8). This suggests that at least some portion of the negative nitrogen concentration anomalies to the south of the KE jet may be explained by the northward migration of the KE jet during the KE stable state.

Although we have focused on the effect of nutrient concentration anomalies, we note that other effects such as MLD variations, light availability, and temperature variations may also influence phytoplankton concentrations. However, it turns out that these effects act as a negative feedback. First, MLD is known to undergo decadal variations associated with the KE state (Sugimoto and Kako 2016) and wintertime MLD anomalies may contribute to nitrogen concentration anomalies because deepening of the mixed layer is associated with entrainment of nutrient-rich subsurface water. However, their contribution seems to not be dominant, as the MLD becomes anomalously deep to the south of the KE jet during the KE stable state (figure not shown), which should favor positive nitrogen concentration anomalies. Also, because of the negative phytoplankton concentration anomalies to the south of the KE jet during stable states, penetrative shortwave radiation anomalies are positive and shortwave radiation can reach deeper (figure not shown). This would favor an increase in phytoplankton concentrations at depth, but the fact that phytoplankton concentration anomalies are negative suggests that the penetrative shortwave radiation anomalies act as a negative feedback, but their impact is smaller compared with the effect of anomalous nutrient concentrations. Furthermore, because of the anomalously deep thermocline, positive temperature anomalies are found to the south of the KE jet (figure not shown). Again, this favors enhanced concentrations of phytoplankton at depth and opposes the negative phytoplankton concentration anomalies associated with reduced nutrient concentration. For more details on their effects, readers may also refer to a paper by Sasai et al. (2022).

Finally, although our analyses have mostly focused on the 145°E section, we present composites of nitrogen and phytoplankton concentration anomalies in February and August that compare cross sections at 142.5°E, 145°E, 147.5°E, and 150°E (Figs. 9 and 10). Negative nitrogen concentration anomalies are found to the south of the KE jet axis from 142.5°E to 150°E with the strongest anomalies at 145°E in both February and August (Fig. 9). In February, strong negative phytoplankton concentration anomalies extending from the surface to about 150 m depth at 142.5°E are further strengthened at 145°E, but

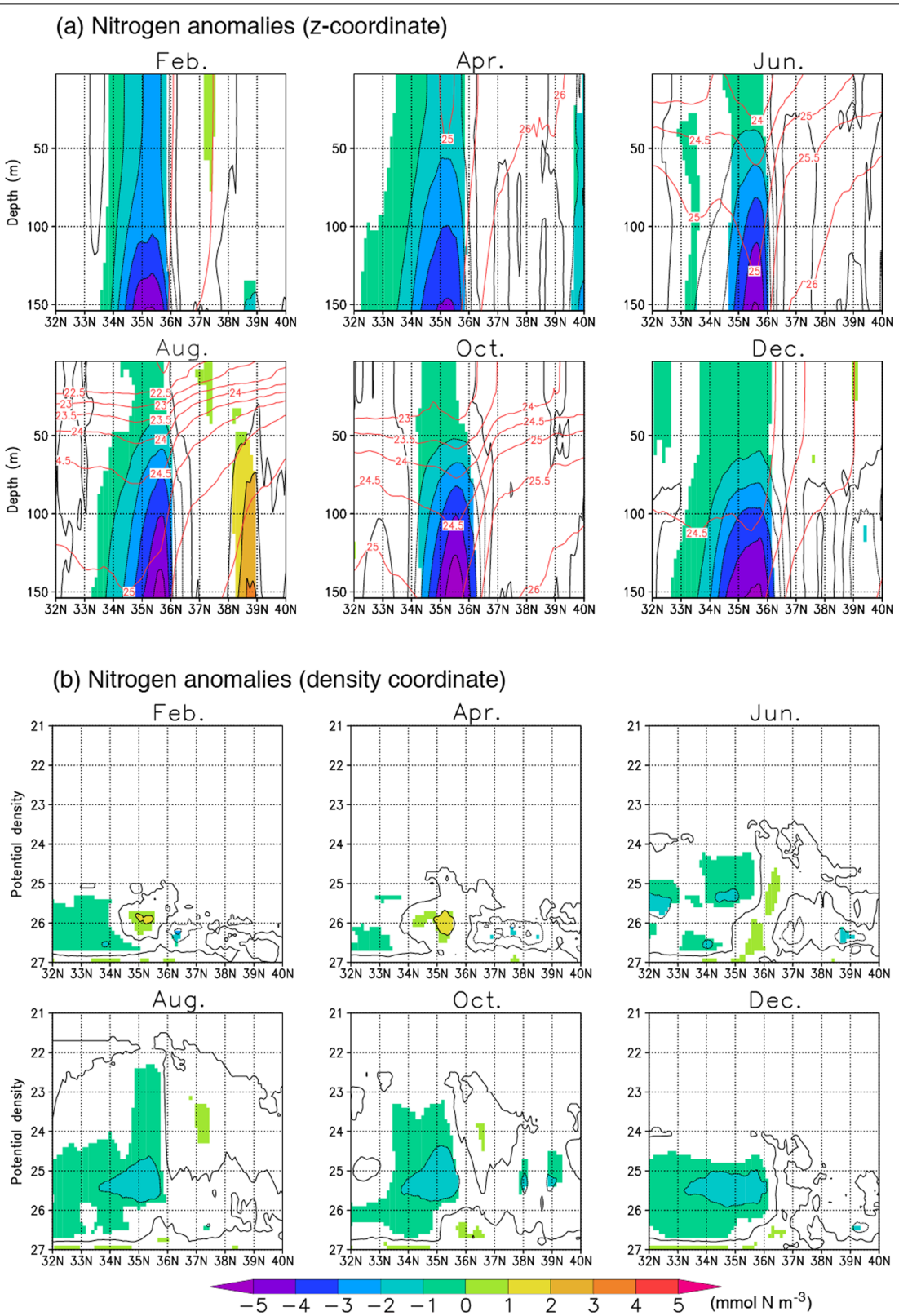

Fig. 7 As in Fig. 5, but for nitrogen concentration anomalies (in mmol N m^{-3}). The black contour intervals are 1 mmol N m^{-3}

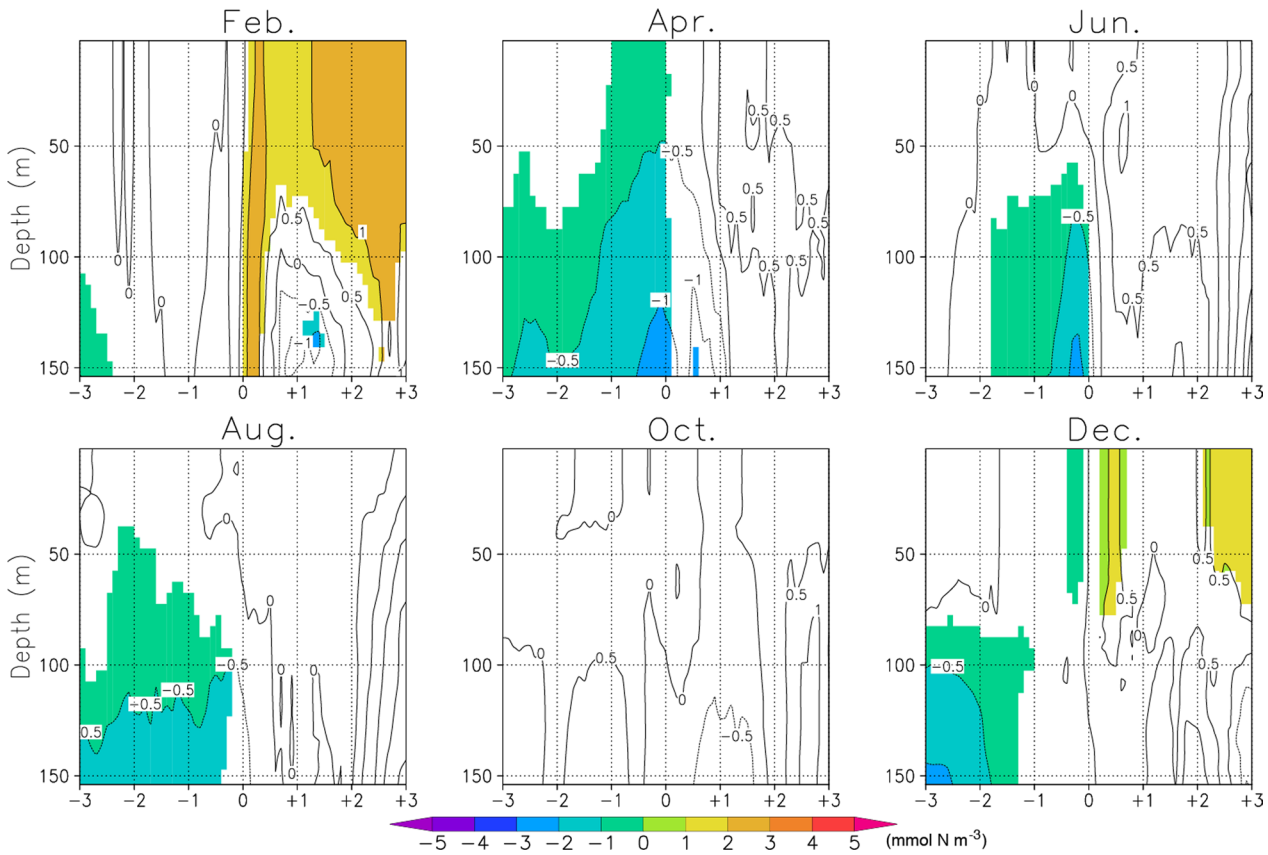

Fig. 8 As in Fig. 7a, but in the KE jet latitude coordinate

weaken gradually from 147.5°E to 150°E (Fig. 10). Since the euphotic layer depth is about 80 m, negative phytoplankton concentration anomalies below this level may be caused by intense wintertime mixing within the mixed layer that extends to about 150 m. In August, the peak negative phytoplankton concentration anomalies found between 24.0 and 24.5 potential density surfaces strengthen from 142.5°E to 145°E, but disappear at 147.5°E and reappear at 150°E (Fig. 10). The disappearance at 147.5°E suggests that the negative phytoplankton concentration anomalies are not just advected zonally by the KE.

4 Conclusions and discussions

In this study, we have investigated decadal variations of phytoplankton concentrations in the upstream KE region using outputs from a simple nitrogen-based NPZD pelagic model embedded in an eddy-resolving ocean general circulation model, which can represent the KE jet and associated frontal structures. Observed seasonal variability in the subsurface structure of Chl-a concentrations and vertical migration of nutricline is also well simulated in the model. In agreement with past studies based on satellite observations and model simulations (Lin et al. 2014, 2020), the surface phytoplankton concentrations are anomalously suppressed to the south of the KE front, while those to the north are anomalously enhanced during winter and spring of the stable state of the KE. However, we have shown for the first time that significant subsurface anomalies centered around 60 m depth persist even in summer and autumn. Although the surface phytoplankton concentration anomalies are prominent only during winter to spring, significant subsurface anomalies centered around 60 m depth persist even in summer and autumn. As a result, significant anomalies exist throughout the year in the phytoplankton biomass integrated over the upper 100 m despite the strong surface anomalies during the spring bloom season. A comparison of nitrogen concentration anomalies in two different coordinate systems suggests that both anomalous vertical movement and mixing contribute to decadal variations in the nitrogen and phytoplankton concentrations. Also, negative nitrogen concentration anomalies to the south of the KE jet associated with stable states of the KE may partially be explained by the northward migration of the

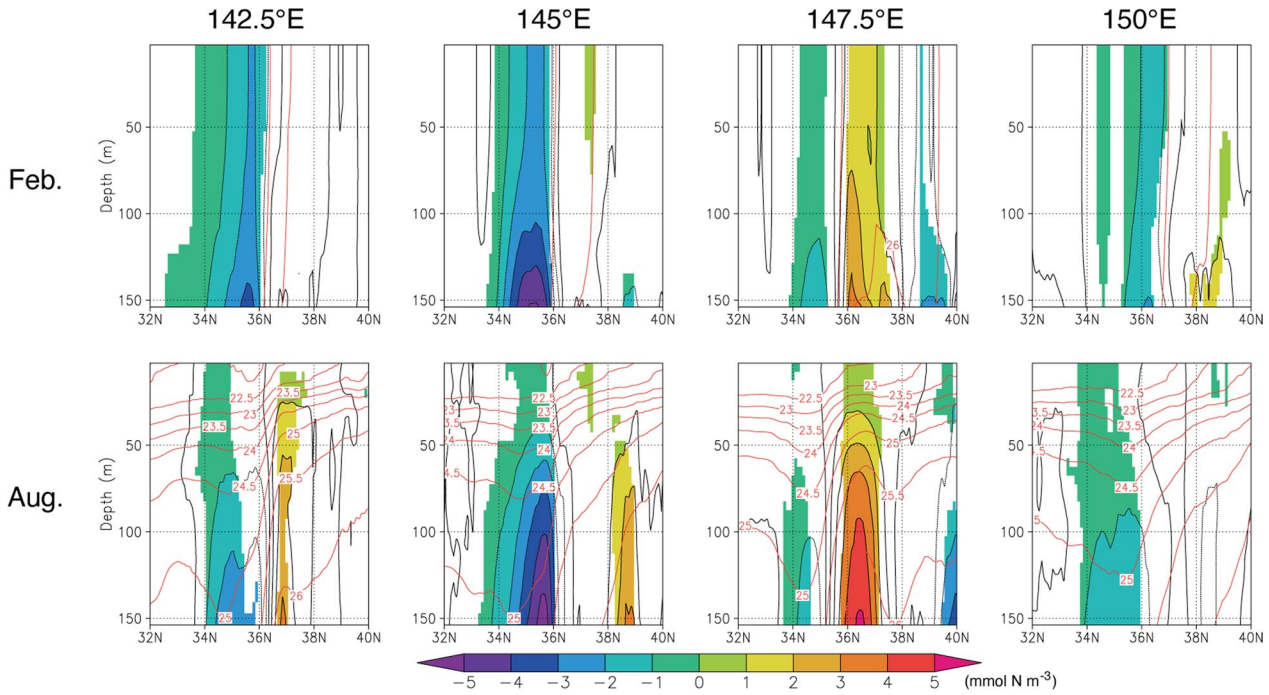

Fig. 9 Composites of nitrogen concentration anomalies (in mmol N m^{-3}) along (left to right) 142.5°E, 145°E, 147.5°E, and 150°E during the stable states in (upper row) February and (bottom row) August. The contour intervals are 1 mmol N m^{-3}. Also shown with red contours are composites of potential density. Anomalies significant at the 95% confidence level by a two-tailed t test are shaded

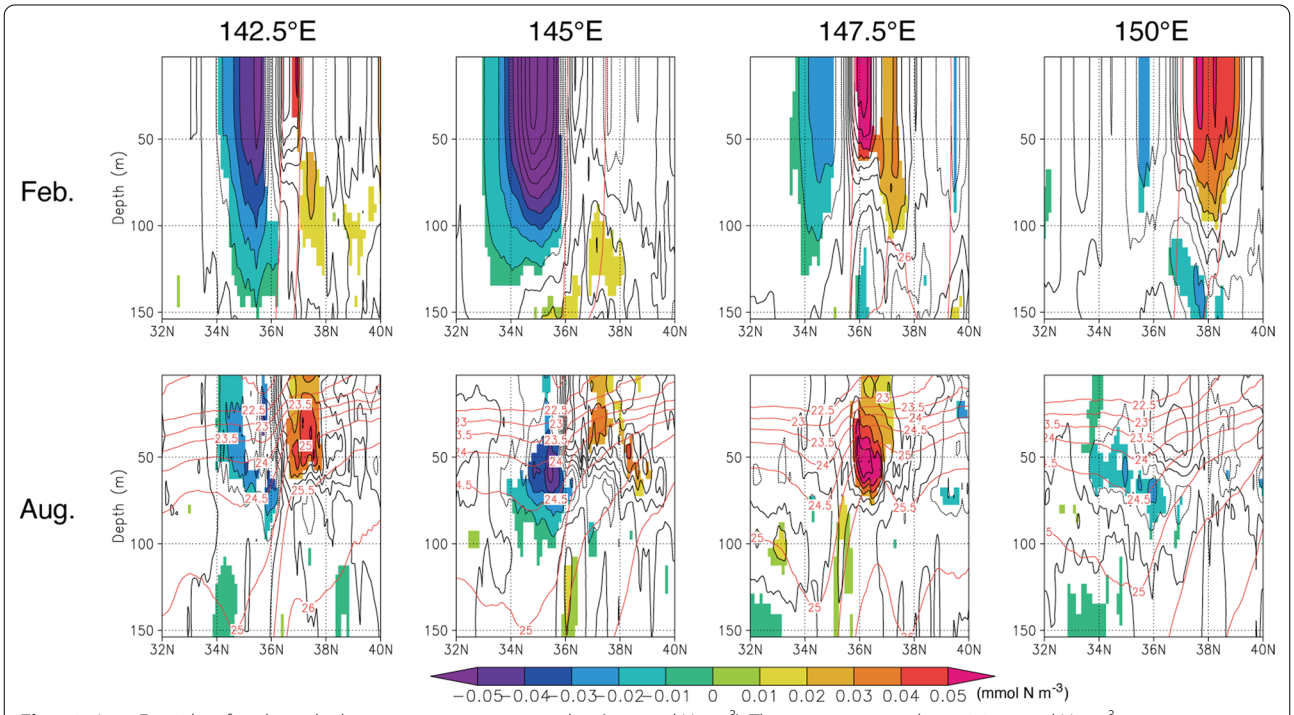

Fig. 10 As in Fig. 9, but for phytoplankton concentration anomalies (in mmol N m^{-3}). The contour intervals are 0.01 mmol N m^{-3}

KE jet, which results in a northward expansion of nutrient poor waters from the subtropical gyre.

Although three possible mechanisms have been proposed, it is difficult to quantify their relative contributions. For example, anomalies in vertical velocity and the latitude of the KE jet axis are negatively correlated with each other. Thus, if we were to quantify their respective contributions with a multiple regression analysis, collinearity becomes an issue. In other words, a northward shift in the KE jet not only leads to a northward extension of nutrient poor waters from the subtropical gyre, but also results in a northward extension of the subtropical gyre associated with downwelling. Another reason is that we do not have the vertical diffusion coefficient as a model output and it is not possible to quantify vertical mixing of nutrients. Conducting an online nitrogen budget analysis (i.e., saving all terms in the nitrogen budget equation at each time step and accumulating them, as was done by Nakazato et al. (2021) for the heat budget equation) may provide a solution.

The KE region is known for its enhanced turbulent diapycnal mixing, and it is attributed to the strong confluence of the Kuroshio and Oyashio currents, and an ageostrophic secondary circulation (D'Asaro et al. 2011; Nagai et al. 2012). The importance of diapycnal mixing suggested by this study is in agreement with Kaneko et al. (2013, 2021), who provided observational evidence that vertical mixing plays an important role in nutrient supply to the euphotic layer.

Although intrinsic variability greatly reduces potential predictability of the KE (Nonaka et al. 2016), westward propagating Rossby waves have been suggested to provide a source of memory for decadal prediction (Qiu et al. 2014; Joh et al. 2022). The relatively high correlations in simulated decadal SSH variations with satellite observations and an ocean re-analysis product (Fig. 3) suggest that decadal variations of phytoplankton concentration in the KE that are closely related to the KE state are potentially predictable.

The region south of the KE is also known as the formation area of the North Pacific subtropical mode water (Masuzawa 1969). Since it is circulated in the western North Pacific (Suga and Hanawa 1995; Suga et al. 2008), decadal variability of phytoplankton concentrations in the KE may have profound impacts on the water properties in vast areas of the western North Pacific (e.g., Oka et al. 2015, 2018) and the uptake of carbon dioxide. Oka et al. (2015) showed some hint of decadal downstream signatures in biogeochemical properties along isopycnal surfaces that correspond to the subtropical mode water, but denser observations and more sophisticated analyses such as water mass transformation diagnostics (e.g., Iudicone et al. 2011) are required to more clearly detect such signatures. Thus, future studies examining the consequence of the decadal variability revealed in this study may further elucidate decadal variability not only in the marine ecosystem in the North Pacific, but also in the oceanic storage of anthropogenic carbon dioxide (Bates et al. 2002).

Mesoscale eddy activity in the KE region is also known to undergo decadal variations with enhanced eddy activity during unstable states and reduced activity during stable states (Qiu and Chen, 2005). Cyclonic eddies to the south of the KE detached from the KE jet have been shown to play an important role in supplying nutrients and enhancing near-surface productivity (Sasai et al. 2010, 2019; Kouketsu et al. 2016; Uchiyama et al. 2017; Honda et al. 2018; Lin et al. 2020). It will be illuminating to investigate how decadal variations in eddy activity associated with the KE state contribute to those in phytoplankton concentrations in the KE region. A study in this direction is underway.

Although the present results are mostly based on modeling, this study suggests the importance of monitoring subsurface phytoplankton variabilities in addition to satellite observations that can measure surface chlorophyll-a concentration. This may be accomplished by expanded deployment of Biogeochemical Argo floats (Bittig et al. 2019).

Abbreviations

Chl-a: Chlorophyll a; EOF: Empirical orthogonal function; FORA-WNP30: Four-dimensional variational ocean re-analysis for the Western North Pacific over 30 years; KE: Kuroshio Extension; GLODAPv2.2019: Global ocean data analysis project version 2.2019 release; MILA GPV: Mixed layer data set of Argo, grid point value; MLD: Mixed layer depth; MRI: Meteorological Research Institute; MRI.COM: Meteorological Research Institute community ocean model; NPZD: Nitrogen, phytoplankton, zooplankton, and detritus; OFES: Ocean general circulation model for the Earth Simulator; PC: Principle component; SSH: Sea surface height; WOA2018: World Ocean Atlas 2018; WOD2018: World Ocean Database 2018.

Acknowledgements

We thank two anonymous reviewers for their constructive comments, which were very helpful in improving our manuscript. The OFES simulation was conducted on the Earth Simulator under the support of JAMSTEC.

Author contributions

TT and YS conceived and designed the study. YS and HS carried out the model simulations. TT and YS analyzed the model outputs, and SY analyzed the observational data. TT wrote the first draft of this manuscript. All authors read and approved the final manuscript.

Funding

This study is supported by the Japan Society for Promotion of Science through Grant-in-Aid for Scientific Research on Innovative Area (MEXT KAKENHI Grant number 19H05701).

Availability of data and material

The outputs from the ecosystem model are available from Yoshikazu Sasai on reasonable request. The satellite altimetry data were obtained from https://cds.climate.copernicus.eu/cdsapp#!/dataset/satellite-sea-level-global, climatological mixed layer depth data were obtained from MILA GPV (http://www.jamstec.go.jp/ARGO/argo_web/argo/?page_id=223andlang=en), and nitrate

concentration data are obtained from the WOA18 (https://www.nodc.noaa.gov/OC5/woa18/). Subsurface chlorophyll a (Chl-a) data were obtained from the WOD2018 (https://www.nodc.noaa.gov/OC5/WOD/pr_wod.html) and the GLODAPv2.2019 (https://www.glodap.info/). Satellite-based PAR and 1% light level depth data were obtained from the GlobColour project website (http://hermes.acri.fr/index.php). This study used the FORA-WNP30, which was produced by Japan Agency for Marine-Science and Technology (JAMSTEC) and Meteorological Research Institute of Japan Meteorological Agency (JMA/MRI) and is available from http://synthesis.jamstec.go.jp/FORA/e/index.html.

Declarations

Competing interests

The authors declare that they have no competing interest.

Author details

[1]Department of Earth and Planetary Science, Graduate School of Science, The University of Tokyo, Tokyo, Japan. [2]Application Laboratory (APL), Research Institute for Value-Added-Information Generation (VAiG), Japan Agency for Marine-Earth Science and Technology (JAMSTEC), Yokohama, Japan. [3]Earth Surface System Research Center, Research Institute for Global Change, JAMSTEC, Yokosuka, Japan. [4]Graduate School of Science, Tohoku University, Sendai, Japan.

Received: 29 June 2022 Accepted: 5 December 2022
Published online: 16 December 2022

References

Bates NR, Pequignet AC, Johnson RJ, Gruber N (2002) A variable sink for atmospheric CO_2 in subtropical mode water of the North Atlantic Ocean. Nature 420:489–493. https://doi.org/10.1038/nature01253

Bittig HC, Mauer TL, Plant JN, Schmechtig C, Wong APS, Claustre H, Trull TW, Udaya Bhaskar TVS, Boss E, Dall'Olmo G, Organelli E, Poteau A, Johnson KS, Hanstein C, Leymarie E, Le Reste S, Riser SC, Rupan AR, Taillandier V, Thierry V, Xing X (2019) A BGC-Argo guide: planning, deployment, data handling and usage. Front Mar Sci 6:502. https://doi.org/10.3389/fmars.2019.00502

Boyer TP, Baranova OK, Coleman C, Garcia HE, Grodsky A, Locarnini RA, Mishonov AV, Paver CR, Reagan JR, Seidov D, Smolyar IV, Weathers K, Zweng MM (2018) World Ocean Database 2018, Mishonov AV, Technical Ed.; NOAA Atlas NESDIS 87, 2018

Chiba S, Di Lorenzo E, Davis A, Keister JE, Taguchi B, Sasai Y, Sugisaki H (2013) Large-scale climate control of zooplankton transport and biogeography in the Kuroshio-Oyashio Extension region. Geophys Res Lett 40:5182–5187. https://doi.org/10.1002/grl.50999

D'Asaro E, Lee C, Rainville L, Harcourt R, Thomas L (2011) Enhanced turbulence and energy dissipation at ocean fronts. Science 332:318–322. https://doi.org/10.1126/science.1201515

Di Lorenzo E, Schneider N, Cobb KM, Franks PJS, Chhak K, Miller AJ, McWilliams JC, Bograd SJ, Arango H, Curchitser E, Powell TM, Rivière P (2008) North Pacific Gyre Oscillation links ocean climate and ecosystem change. Geophys Res Lett 35:L08607. https://doi.org/10.1029/2007GL032838

Frouin R, Franz B, Werdell P (2003) The SeaWiFS PAR product. Algorithm updates for the fourth SeaWIFS data reprocessing, 22, 46–50

Fujiki T, Inoue R, Honda MC, Wakita M, Mino Y, Sukigara C, Abe O (2020) Time-series observations of photosynthetic oxygen production in the subtropical western North Pacific by an underwater profiling buoy system. Limnol Oceanogr 65:1072–1084. https://doi.org/10.1002/lno.11372

Garcia HE, Weathers K, Paver CR, Smolyar I, Boyer TP, Locarnini RA, Zweng MM, Mishonov AV, Baranova OK, Seidov D, Reagan JR (2018) World Ocean Atlas 2018, Volume 4: Dissolved Inorganic Nutrients (phosphate, nitrate and nitrate+nitrite, silicate), Mishonov A Technical Ed.; NOAA Atlas NESDIS 84, 35pp

Honda MC, Sasai Y, Siswanto E, Kuwano-Yoshida A, Aiki H, Cronin MF (2018) Impact of cyclonic eddies and typhoons on biogeochemistry in the oligotrophic ocean based on biogeochemical/physical/meteorological time-series at station KEO. Prog Earth Planet Sci 5:42. https://doi.org/10.1186/s40645-018-0196-3

Hosoda S, Ohira T, Sato K, Suga T (2010) Improved description of global mixed-layer depth using Argo profiling floats. J Oceanogr 66:773–787. https://doi.org/10.1007/s10872-010-0063-3

Itoh S, Yasuda I, Saito H, Tsuda A, Komatsu K (2015) Mixed layer depth and chlorophyll a: Profiling float observations in the Kuroshio-Oyashio Extension region. J Mar Sys 151:1–14. https://doi.org/10.1016/j.jmarsys.2015.06.004

Iudicone D, Rogers KB, Stendardo I, Aumont O, Madec G, Bopp L, Mangoni O, d'Alcala MR (2011) Water masses as a unifying framework for understanding the Southern Ocean carbon cycle. Biogeosci 8:1031–1052. https://doi.org/10.5194/bg-8-1031-2011

Joh Y, Delworth TL, Wittenberg AT, Cooke WF, Yang X, Zeng F, Jia L, Lu F, Johnson N, Kapnick SB, Rosati A, Zhang L, McHugh C (2022) Seasonal-to-decadal variability and prediction of the Kuroshio Extension in the GFDL coupled ensemble reanalysis and forecasting system. J Clim 35:3515–3535. https://doi.org/10.1175/JCLI-D-21-0471.1

Kaneko H, Yasuda I, Komatsu K, Itoh S (2013) Observations of vertical turbulent nitrate flux across the Kuroshio. Geophys Res Lett 40:3123–3127. https://doi.org/10.1002/grl.50613

Kaneko H, Yasuda I, Itoh S, Ito S (2021) Vertical turbulent nitrate flux from direct measurements in the western subarctic and subtropical gyres of the North Pacific. J Oceanogr 77:29–44. https://doi.org/10.1007/s10872-020-00576-0

Kouketsu S, Kaneko H, Okunishi T, Sasaoka K, Itoh S, Inoue R, Ueno H (2016) Mesoscale eddy effects on temporal variability of surface chlorophyll a in the Kuroshio Extension. J Oceanogr 72:439–451. https://doi.org/10.1007/s10872-015-0286-4

Latif M, Barnett TP (1996) Decadal climate variability over the North Pacific and North America: dynamics and predictability. J Clim 9:2407–2423. https://doi.org/10.1175/1520-0442(1996)009%3c2407:DCVOTN%3e2.0.CO;2

Lin P, Chai F, Xue H, Xiu P (2014) Modulation of decadal oscillation on surface chlorophyll in the Kuroshio Extension. J Geophys Res Oceans 119:187–199. https://doi.org/10.1002/2013JC009359

Lin P, Ma J, Chai F, Xiu P, Liu H (2020) Decadal variability of nutrients and biomass in the southern region of Kuroshio Extension. Prog Oceanogr 188:102441. https://doi.org/10.1016/j.pocean.2020.102441

Mantua NJ, Hare SR, Zhang Y, Wallace JM, Francis RC (1997) A Pacific decadal climate oscillation with impacts on salmon. Bull Amer Meteorol Soc 78:1069–1079. https://doi.org/10.1175/1520-0477(1997)078%3c1069:APICOW%3e2.0.CO;2

Masuzawa J (1969) Subtropical mode water. Deep-Sea Res 16:463–472. https://doi.org/10.1016/0011-7471(69)90034-5

Masumoto, Y, Sasaki H, Kagimoto T, Komori N, Ishida A, Sasai Y, Miyama T, Motoi T, Mitsudera H, Takahashi K, Sakuma H, Yamagata T (2004) A fifty-year eddy-resolving simulation of the world ocean—Preliminary outcomes of OFES (OGCM for the Earth Simulator). J Earth Simulator 1:35–56

Morel A, Huot Y, Gentili B, Werdell PJ, Hooker SB, Franz BA (2007) Examining the consistency of products derived from various ocean color sensors in open ocean (Case 1) waters in the perspective of a multi-sensor approach. Remote Sens Environ 111:69–88. https://doi.org/10.1016/j.rse.2007.03.012

Nagai T, Tandon A, Yamazaki H, Doubell MJ, Gallager S (2012) Direct observations of microscale turbulence and thermohaline structure in the Kuroshio Front. J Geophys Res 117:C08013. https://doi.org/10.1029/2011JC007228

Nakazato M, Kido S, Tozuka T (2021) Mechanisms of asymmetry in sea surface temperature anomalies associated with the Indian Ocean Dipole revealed by closed heat budget. Sci Rep 11(1):22546. https://doi.org/10.1038/s41598-021-01619-2

Newman M, Alexander MA, Ault TR, Cobb KM, Deser C, Di Lorenzo E, Mantua NJ, Miller AJ, Minobe S, Nakamura H, Schneider N, Vimont DJ, Phillips AS, Scott JD, Smith CA (2016) The Pacific Decadal Oscillation, revisited. J Clim 29:4399–4427. https://doi.org/10.1175/JCLI-D-15-0508.1

Nonaka M, Nakamura H, Tanimoto Y, Kagimoto T, Sasaki H (2006) Decadal variability in the Kuroshio-Oyashio Extension simulated in an eddy-resolving OGCM. J Clim 19:1970–1989. https://doi.org/10.1175/JCLI3793.1

Nonaka M, Sasai Y, Sasaki H, Taguchi B, Nakamura H (2016) How potentially predictable are midlatitude ocean currents? Sci Rep 6:20153. https://doi.org/10.1038/srep20153

North GR, Bell TL, Cahalan RF, Moeng FJ (1982) Sampling errors in the estimation of empirical orthogonal functions. Mon Wea Rev 110:699–706. https://doi.org/10.1175/1520-0493(1982)110%3c0699:SEITEO%3e2.0.CO;2
Noto M, Yasuda I (1999) Population decline of the Japanese sardine, Sardinops melanostictus, in relation to sea surface temperature in the Kuroshio Extension. Canad J Fish Aquat Sci 56:973–983. https://doi.org/10.1139/f99-028
Oka E, Qiu B, Takatani Y, Enyo K, Sasano D, Kosugi N, Ishii M, Nakano T, Suga T (2015) Decadal variability of subtropical mode water subduction and its impact on biogeochemistry. J Oceanogr 71:389–400. https://doi.org/10.1007/s10872-015-0300-x
Oka E, Yamada K, Sasano D, Enyo K, Nakano T, Ishii M (2018) Remotely forced decadal physical and biogeochemical variability of North Pacific subtropical mode water over the last 40 years. Geophys Res Lett 46:1555–1561. https://doi.org/10.1029/2018GL081330
Olsen A, Lange N, Key RM, Tanhua T, Álvarez M, Becker S, Bittig HC, Carter BR, Cotrim da Cunha L, Feely RA, van Heuven S, Hoppema M, Ishii M, Jeansson E, Jones SD, Jutterström S, Karlsen MK, Kozyr A, Lauvset SK, Lo Monaco C, Murata A, Pérez FF, Pfeil B, Schirnick C, Steinfeldt R, Suzuki T, Telszewski M, Tilbrook B, Velo A, Wanninkhof R (2019) GLODAPv2.2019—An update of GLODAPv2. Earth Syst Sci Data 11:1437–1461. https://doi.org/10.5194/essd-11-1437-2019
Oschlies A, Koeve W, Garçon V (2000) An eddy-permitting coupled physical-biological model of the North Atlantic: 2. Ecosystem dynamics and comparison with satellite and JGOFS local station data. Global Biogeochem Cycle 14:499–523. https://doi.org/10.1029/1999GB900080
Pastor MV, Palter JB, Pelegrí JL, Dunne J (2013) Physical drivers of interannual chlorophyll variability in the eastern subtropical North Atlantic. J Geophys Res Oceans 118:3871–3886. https://doi.org/10.1002/jgrc.20254
Qiu B, Chen S (2005) Variability of the Kuroshio Extension jet, recirculation gyre, and mesoscale eddies on decadal time scales. J Phys Oceanogr 35:2090–2103. https://doi.org/10.1175/JPO2807.1
Qiu B, Chen S, Schneider N, Taguchi B (2014) A coupled decadal prediction of the dynamic state of the Kuroshio Extension system. J Clim 27:1751–1764. https://doi.org/10.1175/JCLI-D-13-00318.1
Sasai Y, Ishida A, Sasaki H, Kawahara S, Uehara H, Yamanaka Y (2006) A global eddy-resolving coupled physical and biological model: Physical influences on a marine ecosystem in the North Pacific. SIMULATION 82:467–474. https://doi.org/10.1177/0037549706068943
Sasai Y, Sasaoka K, Sasaki H, Ishida A (2007a) Seasonal and intraseasonal variability of chlorophyll-a in the North Pacific: Model and satellite data. J Earth Simulator 8:3–11
Sasai Y, Sasaki H, Sasaoka K, Ishida A, Yamanaka Y (2007b) Marine ecosystem simulation in the eastern tropical Pacific with a global eddy resolving coupled physical-biological model. Geophys Res Lett 34:L23601. https://doi.org/10.1029/2007GL031507
Sasai Y, Richards KJ, Ishida A, Sasaki H (2010) Effects of cyclonic mesoscale eddies on the marine ecosystem in the Kuroshio Extension region using an eddy-resolving coupled physical-biological model. Ocean Dyn 60:693–704. https://doi.org/10.1007/s10236-010-0264-8
Sasai Y, Smith SL, Siswanto E, Sasaki H, Nonaka M (2022) Physiological flexibility of phytoplankton impacts modeled biomass and primary production across the North Pacific Ocean. Biogeosci 19:4865–4882. https://doi.org/10.5194/bg-19-4865-2022
Sasai Y, Honda MC, Siswanto E, Kato S, Uehara K, Sasaki H, Nonaka M (2019) Impact of ocean physics on marine ecosystems in the Kuroshio and Kuroshio Extension regions: A high-resolution coupled physical-biological model study. In: Nagai T, Saito H, Suzuki K, Takahashi M. (eds) Kuroshio Current: Physical, Biogeochemical and Ecosystem Dynamics. AGU Geophysical Monograph Series. AGU-Wiley, pp 175–188. https://doi.org/10.1002/9781119428428.ch11
Sasaki YN, Schneider N (2011) Decadal shifts of the Kuroshio Extension jet: application of thin-jet theory. J Phys Oceanogr 41:979–993. https://doi.org/10.1175/2011JPO4550.1
Sasaki YN, Minobe S, Schneider N (2013) Decadal response of the Kuroshio Extension jet to Rossby waves: observation and thin-jet theory. J Phys Oceanogr 43:442–456. https://doi.org/10.1175/JPO-D-12-096.1
Sasaki H, Kida S, Furue R, Aiki H, Komori N, Masumoto Y, Miyama T, Nonaka M, Sasai Y, Taguchi B (2020) A global eddying hindcast ocean simulation with OFES2. Geosci Model Develop 13:3319–3336. https://doi.org/10.5194/gmd-13-3319-2020
Suga T, Hanawa K (1995) The subtropical mode water circulation in the North Pacific. J Phys Oceanogr 25:958–970. https://doi.org/10.1175/1520-0485(1995)025%3c0958:TSMWCI%3e2.0.CO;2
Suga T, Aoki Y, Saito H, Hanawa K (2008) Ventilation of the North Pacific subtropical pycnocline and mode water formation. Prog Oceanogr 77:285–297. https://doi.org/10.1016/j.pocean.2006.12.005
Sugimoto S, Kako S (2016) Decadal variation in winter mixed layer depth south of the Kuroshio Extension and its influence on winter mixed layer temperature. J Clim 29:1237–1252. https://doi.org/10.1175/JCLI-D-15-0206.1
Taguchi B, Xie SP, Schneider N, Nonaka M, Sasaki H, Sasai Y (2007) Decadal variability of the Kuroshio Extension: observations and an eddy-resolving model hindcast. J Clim 20:2357–2377. https://doi.org/10.1175/JCLI4142.1
Tozuka T, Cronin MF, Tomita H (2017) Surface frontogenesis by surface heat fluxes in the upstream Kuroshio Extension region. Sci Rep 7:10258. https://doi.org/10.1038/s41598-017-10268-3
Tsujino H, Usui N, Nakano H (2006) Dynamics of Kuroshio path variations in a high-resolution GCM. J Geophys Res Oceans 111:C11001. https://doi.org/10.1029/2005JC003118
Tsujino H, Urakawa S, Nakano H, Small RJ, Kim WM, Yeager SG, Danabasoglu G, Suzuki T, Bamber JL, Bentsen M, Böning CW, Bozec A, Chassignet EP, Curchitser E, Dias FB, Durack PJ, Griffies SM, Harada Y, Ilicak M, Josey SA, Kobayashi C, Kobayashi S, Komuro Y, Large WG, Le Sommer J, Marsland MJ, Masina S, Scheinert M, Tomita H, Valdivieso M, Yamazaki D (2018) JRA-55 based surface dataset for driving ocean-sea-ice models (JRA55-do). Ocean Model 130:79–139. https://doi.org/10.1016/j.ocemod.2018.07.002
Uchiyama Y, Suzue Y, Yamazaki H (2017) Eddy-driven nutrient transport and associated upper-ocean primary production along the Kuroshio. J Geophys Res Oceans 122:5046–5062. https://doi.org/10.1002/2017JC012847
Usui N, Fujii Y, Sakamoto K, Kamachi M (2015) Development of a four-dimensional variational assimilation system for coastal data assimilation around Japan. Mon Wea Rev 143:3874–3892. https://doi.org/10.1175/MWR-D-14-00326.1
Usui N, Wakamatsu T, Tanaka Y, Hirose N, Toyoda T, Nishikawa S, Fujii Y, Takatsuki Y, Igarashi H, Nishikawa H, Ishikawa Y, Kuragano T, Kamachi M (2017) Four-dimensional variational ocean reanalysis: a 30-year high-resolution dataset in the western North Pacific (FORA-WNP30). J Oceanogr 73:205–233. https://doi.org/10.1007/s10872-016-0398-5
Yasunaka S, Ono T, Sasaoka K, Sato K (2022) Global distribution and variability of subsurface chlorophyll a concentration. Ocean Sci 18:255–268. https://doi.org/10.5194/os-18-255-2022

Publisher's Note